Nanoscale

Accepted Manuscript

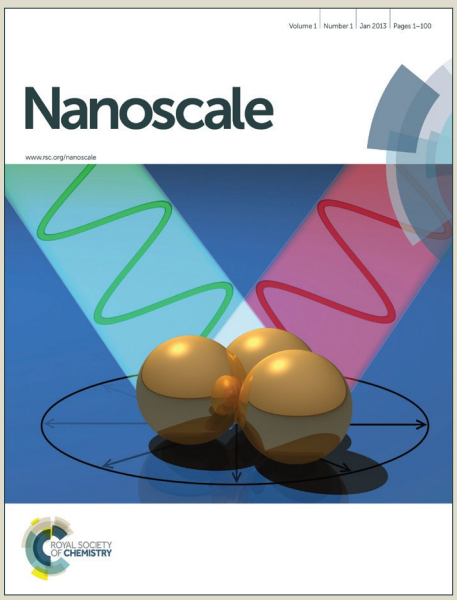

ROYAL SOCIETY OF CHEMISTRY

www.rsc.org/nanoscale

Characteristics of localized surface plasmons excited on mixed monolayers composed of self-assembled Ag and Au nanoparticles

*Daisuke Tanaka[1], Keisuke Imazu[2], Jinwoo Sung[3], Cheolmin Park[3], Koichi Okamoto[2], and Kaoru Tamada[2]**

[1] *Department of Electrical and Electronic Engineering*
National Institute of Technology, Oita College
1666 Maki, Oita 870-0152, Japan

[2] *Institute of Materials Chemistry and Engineering (IMCE)*
Kyushu University
744 Motooka, Nishi-ku, Fukuoka 819-0395, Japan

[3] *Department of Materials Science and Engineering*
Yonsei University,
50 Yonsei-ro, Seodaemun-gu, Seoul 120-749, Korea

E-mail: tamada@ms.foc.kyushu-u.ac.jp

Keywords: metal nanoparticles, mixed monolayer, self-assembly, localized surface plasmons, FDTD simulation

Abstract

The fundamental characteristics of localized surface plasmon resonance (LSPR) excited on mixed monolayers composed of self-assembled Ag and Au nanoparticles (AgNPs and AuNPs, respectively) were investigated. Mixed monolayer films were fabricated at the air-water interface at different mixing ratios. The films retained their phase-segregated morphologies in which AuNPs formed several 10- to 100-nm island domains in a homogeneous AgNP matrix phase. The LSPR bands originating from the self-assembled domains shifted to longer wavelengths as the domain size increased, as predicted by a finite-difference time-domain (FDTD) simulation. The FDTD simulation also revealed that even an alternating-lattice-structured two-dimensional (2D) AgNP/AuNP film retained two isolated LSPR bands, revealing that the plasmon resonances excited on each particle did not couple even in a continuous 2D sheet, unlike in the homologous NP system. The fluorescence

quenching test of Cy3 and Cy5 dyes confirmed that the independent functions of AuNPs and AgNPs remained in the mixed films, whereas the AuNPs exhibited significantly higher quenching efficiency for the Cy3 dye compared with AgNPs due to the overlap of the excitation/emission bands of the dyes with the AuNP LSPR band. Various applications can be considered using this nanoheterostructured plasmonic assembly to excite spatially designed, high-density LSPR on macroscopic surfaces.

1. Introduction

Metallic nanoparticles (NPs) and related topics have been rapidly developing research fields in recent years, and a variety of NPs have been synthesized for various applications.[1-5] Localized surface plasmon resonance (LSPR) excited on novel metal NPs are one of the representative functions originating from nanostructures, which can be widely utilized for various devices to improve their optical or optoelectronic properties.[6-11] Tuning the LSPR bands is an important issue for these device applications, especially those on a wide solid substrate, to secure the quality of the device functions.[12]

In our previous study, we tuned the LSPR bands on a wide surface using self-assembled AgNPs fabricated at the air-water interface.[13,14] Using this technique, the two-dimensional (2D) crystalline AgNP sheets with a constant gap distance, achieved via organic capping molecules, are easily and reproducibly transferred onto hydrophobic solid substrates. This sheet exhibits sharp LSPR bands, which are narrower than those in a dispersion solution.

The FDTD simulation study revealed that the *macroscopic* size of the domains is key for determining the LSPR band position, along with the size and shape of the individual particles and the gap distances.[13] For the case of AgNPs with a 5-nm diameter, our calculation predicted that a domain of more than 200 nm (30 particles in one direction) needs to be treated as a *macroscopic* domain in which the LSPR band shift, which depends on the domain size, is saturated. This phenomenon correlated with the excitation of the low-wave vector

(propagation) mode on AgNP 2D sheets, along with the high-wave vector (LSPR) mode on the individual AgNPs. The half wavelength of this propagation wave is approximately 200 nm. When the size of the domains is larger than 200 nm, homogeneous excitation of the LSPR (‘*delocalized*’ LSPR) is expected, which leads to extraordinary macroscopic optical properties of the AgNP 2D sheets.

In this study, we demonstrated the theoretical prediction described above (domain size-dependent LSPR band shift) experimentally using AgNP and AuNP mixed monolayers. In this study, a one-to-one correspondence between the domain size and the LSPR band position was studied. The interparticle interaction between heterogeneous AgNPs and AuNPs was investigated using FDTD simulations.

We also evaluated the fluorescence quenching efficiency of AgNPs and AuNPs in the mixed monolayers to determine whether their independent functions remained in the mixed films. Cy3 and Cy5 were utilized as fluorescent dyes in which the excitation/emission spectra of the Cy3 dye had a larger overlap with the LSPR band of AuNPs compared with other combinations.

These studies are important for the design and handling of *complex* metal NP-originating nanoarchitectures and their LSPR field for use in future plasmon-originating optical or optoelectronic devices.[15]

2. Experimental

The transmission UV-Vis absorption spectra at the air-water interface were obtained using a multi-channel array spectrometer (MCPD-9800, Otsuka Electronics Co., Ltd., Japan) with a mirror at the bottom of the Langmuir-Blodgett (LB) trough. The spectra of the transferred film on quartz were obtained using a UV-Vis spectrometer (UV-1800, Shimadzu). SEM images were obtained with a HITACHI High-Technologies SU8000 scanning electron microscope.

FDTD simulations were conducted using commercial software (Poynting for Optics, Fujitsu, Japan). A model of AgNP and AuNP mixed sheets was described based on the experimental system, i.e., 5-nm AgNPs and 10-nm AuNPs or 5-nm AgNPs and 5-nm AuNPs, both of which are in a hexagonally packed structure. Interparticle distances are assumed to be 2 nm for 5-nm particles and 3 nm for 10-nm particles. The dielectric function of Ag was approximated by the Drude formula as previously reported.[13] The dielectric function of Au is known to be difficult to describe with the simple Drude formula.[16] However, because the FDTD calculation becomes highly complicated and unstable with the Drude-Lorentz formula, we performed the FDTD simulations of Au using the Drude formula in the same manner described in the previous report.[16] The FDTD simulation with this simplified model of Au is known to be still available at least for the wavelength range from 500 nm to 1000 nm.

An epifluorescence microscope (ECLIPSE 80i, Nikon, Japan) was used to determine the fluorescence intensity from the Cy3 and Cy5 dyes on the AgNP/AuNP mixed film. An excitation wavelength of 510 to 560 nm was utilized for Cy3, while 630 to 650 nm was utilized for Cy5. The light source was a filtered mercury lamp (CLHG1 100 W, Nikon, Japan). Fluorescence images of Cy3 were obtained through a long-pass filter (590 nm), while those of Cy5 were obtained with a band-pass filter (658 to 694 nm). The exposure time for the CCD camera was 3 sec for all of the experiments. The fluorescence intensities on the NP sheets were calibrated by the intensity measured on regular glass substrates.

3. Results and Discussions

3.1 Fabrication of AgNP and AuNP mixed monolayers

Myristate-capped silver nanoparticles (AgNPs, 5 nm in diameter) were synthesized via thermal reduction, as described in our previous study.[13] Oleylamine-capped gold nanoparticles (AuNPs, 10 nm in diameter) were synthesized according to the procedure reported in a previous study.[17] Dodecanethiol-capped gold nanoparticles (AuNPs, 5 nm in diameter) were also synthesized by a two-phase Brust's reduction method as described

previously.[18] Mixed monolayers were fabricated by spreading a mixed solution of AgNPs and AuNPs in toluene at the air-water interface followed by the spontaneous self-assembly on a LB trough (KSV Mini-trough 2000). The film compositions (Ag:Au = 1:9, 2:8, 3:7, 5:5, 7:3, 8:2 and 9:1) were controlled by the mixing ratio of AgNPs and AuNPs in solution. These ratios were defined by the 'occupied area' on water by each NP component, which was calculated from the 'area per particle', as determined from the surface pressure (Π) - Area (A) curves of single component NP.

Figure 1 shows the Π-A curves of mixed 5-nm AgNP and 10-nm AuNP films. As reported in our previous study, the single components of AgNPs and AuNPs form solid-like films, and their surface pressures are not considered to be in equilibrium.[13] The Π-A profiles near the lift-up point are unstable (low reproducibility) for the single component and the mixed films. However, the averaged 'area per particle' value obtained by the extrapolation of the linear region (i.e., 10 mN/m$\leqq$Π$\leqq$15 mN/m) exhibited nearly ideal mixing. These data suggest that mixed AgNPs and AuNPs formed monolayers.

Figure 2 illustrates the transmission absorption spectra of 5-nm AgNPsand 10-nm AuNP mixed films measured at the air-water interface (a) and on hexamethyldisilazane (HMDS)-treated hydrophobic quartz at Π = 15 mN/m (b). The spectra were normalized by taking the main peak intensity as unity. Both of the spectra in Figure 2(a) and (b) exhibit the same general tendency; the band position of AgNPs does not substantially change due to mixing, while that of AuNPs shows a significant redshift as the number of AuNPs increases. We also confirmed an additional redshift of the LSPR bands on quartz compared with those on water, which is discussed along with the SEM images in the following section.

Figure 3 shows the representative SEM images of single component 5-nm AgNP and 10-nm AuNP monolayers transferred onto hydrophobic Si-wafers at Π = 15 mN/m. The AgNPs form a more homogeneous, continuous film compared with AuNPs. The AuNP film is composed of round domains, which must be formed at the initial stage of self-assembly, i.e.,

the spreading and drying process of the AuNP solution at the air-water interface. It is known that AgNPs also form solid-like domains when spread on water, as reported in our previous study; however, the domains are merged into one continuous monolayer sheet by compression due to their two-dimensional plasticity.[13] In contrast, AuNP domains apparently do not deform during the compression process because of their rigidity.[17] Thus, AgNPs and AuNPs possess different viscoelastic properties, possibly because of the different attraction forces between the particles. Although the capping organic molecules are different (myristate or oleylamine), we hypothesize that the size of the particles (i.e., 5-nm AgNPs and 10-nm AuNPs) was more critical for determining their properties. The van der Waals force between spherical particles is approximated using a relatively simple equation with the Hamaker constant (A) when the particles are sufficiently large (diameter: R_1 or R_2) compared with the gap distance (D), i.e., $D << R_1$ or R_2, as follows:[19]

$$F_{vw} = -\frac{A}{6D^2}\left(\frac{R_1 R_2}{R_1 + R_2}\right) \quad (1)$$

The Hamaker constants of Ag and Au are known to be comparable (Ag: 50 x10^{-20} J in vacuum and 40 x10^{-20} J in water, Au: 40 x10^{-20} J in vacuum and 30 x10^{-20} J in water).[20] However, the size of the particles is different by two-fold between AgNPs and AuNPs. The simple calculation in eq. (1) gives approximately a 1.5 times stronger force between AuNPs and AuNPs compared with that between AgNPs and AgNPs. Because the size distribution of AuNPs is relatively large, we can observe that the larger-sized AuNPs are assembled at the centre of the domains (possibly assembled first) and are then surrounded by smaller-sized AuNPs (Fig. 3(b)), providing evidence that the particle size influences the self-assembly.

The morphological observation of AgNP and AuNP mixed films shown in **Figure 4** confirmed our hypothesis that AuNPs formed island domains and AgNPs surrounded the AuNP domains like a matrix material in all cases. The AuNP domain size depends on the mixing ratio, which increases as the number of AuNPs increases in the mixture.

Figure 5 shows SEM images of 5-nm AgNP and 5-nm AuNP mixed films (Ag:Au = 3:7, 5:5, and 7:3) for comparison. **Figure 6** shows the normalized transmission absorption spectra of the 5-nm AgNP and 5-nm AuNP mixed films on water (a) and on quartz substrates (b). In the SEM images, the AuNPs appeared as brighter dots, while the AgNPs appeared as darker dots. When the particle sizes of the AgNPs and AuNPs are the same (both are 5 nm in diameter), they are random mixtures (Fig. 5b), in a similar manner to the binary 2D self-assembly of proteins.[21] Eventually, for the Ag:Au = 3:7 mixtures, the minor ingredient (AgNPs) formed island-like domains, and the main ingredient (AuNPs) formed the matrix phase shown in Figure 5a. When the mixing ratio was inverted (Ag:Au = 7:3), the image was inverted, as shown in Figure 5c. Thus, the morphologies of the 5-nm AgNP and 5-nm AuNP mixed films were significantly different from those of the 5-nm AgNP and 10-nm AuNP mixed films, which supported our hypothesis that the self-assembled structures of 2D metal NP sheets were mainly determined by their particle sizes. The absorption spectra of the 5-nm AgNP and 5-nm AuNP mixed films shown in Figure 6 are consistent with their film morphologies, in which not only AuNPs but also AgNPs show significant peak shifts due to the mixing ratio, indicating the change in domain size.

Figure 7 summarizes the AgNP and AuNP LSPR peak positions in mixed films on water and on quartz substrates. The data are derived from Figure 2 and Figure 6. It is interesting that the film transfer from the water surface to the quartz substrate induced the additional redshift only for the 5-nm AgNP and 10-nm AuNP mixed system (especially for the LSPR peaks originating from the AuNPs). This phenomenon must be related to how *tight* the original self-assembled structure is on the water surface. In fact, the SEM images in Figure 5 revealed densely packed, crystalline films composed of AgNPs and AuNPs of the same size. This rigid self-assembled structure seems to be assembled during the solvent evaporation process, and further rearrangement of the particles must be difficult after the film is made. On the other hand, for the 5-nm AgNP and 10-nm AuNP system, there must be a certain level of

geometrical defects at the domain boundary originating from lattice mismatch (the model for the FDTD simulation in Figure 9 shows a view of the defects at the domain boundary, as one example), which may have contributed to the rearrangement of the particles later on. The defects originating from the size distribution of the 10-nm AuNPs may also have participated in this phenomenon. In any case, the incomplete self-assembly on the water surface must be the origin of the further redshift upon transfer to the solid substrate.

3.2 FDTD simulation of AgNP and AuNP mixed films

Figure 8 shows the correlation between the LSPR band positions originating from 5-nm AgNPs and 10-nm AuNPs, extracted from Fig. 2b, and the size of the domains measured from the SEM images shown in Fig. 4. The size of the domains is defined as schematically described in Fig. 8. In the case of AuNPs, the diameter of the island domain is measured as the AuNP domain size. In contrast, the average distance between neighbouring AuNP islands is regarded as the AgNP domain size (i.e., the 'size' of the matrix phase). For both cases, as the domain size increases, the LSPR peak position is redshifted; thus, a positive correlation was confirmed between these parameters.

In our previous study, we investigated the correlation between the LSPR band position and the number of particles participating in self-assembly for 1D and 2D systems.[13] The FDTD simulation using a model of 5-nm AgNP sheet revealed a significant redshift in both the 1D and 2D systems as the number of 5-nm AgNPs increased, which reached saturation at 10 particles for the 1D system and 30 particles for the 2D system (for the calculation of the 2D system, only the number of particles on the **X**-axis is increased, while a periodic boundary condition was set on the **Y**-axis; the irradiated light was polarized with respect to the **X**-axis). The calculation for the AuNP 2D film gave the same general result, which is available in the supporting information.

In this study, we conducted an FDTD simulation for 5-nm AgNP and 10-nm AuNP mixed films with the model described based on the SEM images of the mixed films, as shown in **Figure 9**. Hexagonally packed island domains composed of different numbers of 10-nm AuNPs (with 3-nm gap distances) were located in the centres of the unit cells, which were surrounded by hexagonally packed 5-nm AgNPs with 2-nm gap distances (AuAg1, AuAg2, AuAg3, and AuAg4). Here, we note that the boundary between the AuNP island domain and the AgNP matrix phase includes an additional maximum gap of a few nanometres in places due to geometrical defects caused by lattice mismatch, even for the optimized densely arranged structures (the nearest neighbour distance between AgNPs and AuNPs was 3 nm). The **X**- and **Y**-axes were set as periodic boundaries. The light polarized along the **X**-axis was irradiated from the backside of the film, and a transmitted light detector was placed at the front side, 12 nm from the centre plane. The optical parameters for the FDTD simulation and the results are shown in **Figure 10**. The experimental results were reproduced by the simulation in which the LSPR band of the AuNPs forming island domains exhibited a larger redshift (533 nm to 584 nm) compared with that of the AgNP matrix phase (462 nm to 467 nm). In addition, the absolute LSPR wavelengths obtained from the simulation are not markedly different from the experimental values, although the simple Drude model was used to reconstruct the dielectric constant of these particles.

After observation of the two peaks originating from AuNPs and AgNPs in the experiment and in the simulation, the question arose of whether the LSPR band of adjacent AuNPs and AgNPs could couple. The AuAg6 model in **Figure 11** answered this question. In this model, 5-nm AuNPs and 5-nm AgNPs were aligned alternately with a 2-nm gap (no defects at the AgNP-AuNP boundary). The spectrum obtained by the FDTD simulation is shown in Figure 11(right). Even when all of the particles were adjacent to different types of particles, two clear peaks were confirmed. Although the respective LSPR peaks did not merge, the neighbouring particles (their LSPR field or their dielectric constant) must influence these bands. To confirm

this idea, we performed the following simulation with the model shown in **Figure 12**. The different types of single particles (5 nm in diameter) were located in a hexagonally packed 2D sheet (Model AuAg7-1 and AuAg7-2), and the wavelength-dependent local field intensity at each gap position (points 1 - 6) was calculated to predict the 'local' LSPR spectra in nanospace. The simulation results revealed that the influence of a single AuNP reached to only the 2nd or 3rd neighbouring AgNPs in the 2D sheet (AuAg7-1, experimental model). Similarly, the influence of a single AgNP reached to only the 2nd or 3rd neighbouring AuNPs in the AuNP 2D sheet (AuAg7-2, inversion model). We changed the size of the foreign (single) NPs from 5 nm to 10 nm to examine the influence of particle size; however, the results showed no difference.

3.3 Fluorescence quenching on AgNP and AuNP mixed monolayers

Fluorescence quenching is a useful tool for highly sensitive biosensing and imaging. [22,23] When a fluorescence dye is placed near a metal NP, the fluorescence emission can be quenched and/or enhanced depending on the experimental conditions, especially depending on the distance between the dye and the particle in nanospace. [24,25] The LSPR field excitation on metal particles, which contributes to fluorescence enhancement (radiative process), rapidly decays as the distance from the surface increases (i.e., the decay length changes according to the size of the metal particles). Förster resonance energy transfer (FRET), which contributes to fluorescence quenching (non-radiative process), also decays with the distance from the surface.[26] Because these phenomena exhibit a trade-off relationship with a similar decay length, a separation distance that differs by a few nanometres could result in both enhancement and quenching. In our previous study, we achieved fluorescence enhancement on 5-nm AgNP sheets using a 20-nm-thick SiO_2 spacer layer between the dye and particle.[27] In this study, we constructed a system suitable for fluorescence quenching with a 5-nm-thick SiO_2 spacer layer and investigated the quenching efficiency of 5-nm AgNPs and 10-nm

AuNPs in the mixed monolayers.

Fluorescence quenching experiments were conducted with Cy3- and Cy5-labelled streptavidin (Amersham) immobilized homogeneously on AgNP and AuNP mixed films.[28] For the measurements, AgNP/AuNP mixed films were coated with SiO_2 sputtered film (5-nm-thick), and then, 3-aminopropyltriethoxysilane (APTES, Sigma-Aldrich) and biotin-PEG-carbonate-NHS (SUNBRIGHT BI-050TS, NOF) were introduced to immobilize dye-labelled streptavidin via biotin-avidin interactions. **Figure 13(a)** shows the epifluorescence microscopy images of Cy3 and Cy5 on the AgNP/AuNP mixed monolayers. **Figure 13(b)** summarizes the relative fluorescence intensity (the intensity on a glass substrate is taken as one) against the occupied area of AuNPs. The open and closed squares indicate the data for Cy3 (2 series of experiments), while the open and closed circles indicate the data for Cy5 (2 series of experiments).

In the case of Cy3, as the occupied area of AuNPs increased from 0% to 50%, the fluorescence intensity rapidly attenuated, and it reached close to zero at 50% (perfect quenching). The profile exhibited a certain threshold at approximately 50% occupied area of AuNP. In contrast, the fluorescence intensity of Cy5 attenuated only slightly and linearly with the mixing ratio of AuNPs and AgNPs.

These results indicate several important characteristics concerning fluorescence quenching (and enhancement) by metal NPs. **Figure 14** explains the overlap of the LSPR band of AgNP and AuNP sheets and the Ag:Au = 5:5 mixed film with the excitation (Ex) and emission (Em) spectra of Cy3 and Cy5. The Ex/Em spectra of Cy3 (559 nm / 568 nm) have a small overlap with the LSPR band of AgNPs in the long wavelength region, while they have significant overlap with that of AuNPs, especially in the 5:5 mixed film ('blueshifted' peak position due to the domain size effect; see Figure 2). The Ex/Em spectra of Cy5 (650 nm / 670 nm) have no overlap with the LSPR band of AgNPs, while their overlap with the LSPR band of AuNPs decreases linearly as the mixing ratio of AuNPs decreases.

Our experimental results revealed that the overlap between the Ex/Em spectra of the fluorescent dye and the LSPR band greatly affected the fluorescence quenching (and enhancement) efficiency.[29-31] The AuNPs maintained a high quenching capacity against the Cy3 dye compared with the other combinations. The threshold at the 50% occupied area that was detected in the plot of Fig. 10 is reasonably interpreted by the efficient spectra overlap of Em(Cy3) with the LSPR band of AuNPs due to the 'blueshift' of the LSPR band caused by mixing. The slightly stronger fluorescence of Cy3 compared with Cy5 on the 100% AgNP sheet, which contributes to the 'high contrast' of the Cy3 fluorescence intensity above and below the 50% threshold, is most likely due to the LSPR-enhanced fluorescence caused by the overlap of Ex (Cy3) with the LSPR band of AgNPs.

Consequently, AuNPs distributed in the mixed films could quench twice as much surface area composed of Cy3 compared with Cy5, and the data demonstrated that the characteristics of the LSPR band of AuNP remained in the AuNP and AgNP mixed monolayers.

4. Conclusion

In this study, we investigated the fundamental characteristics of LSPR excited on AgNP and AuNP mixed 2D sheets. The colour and spectrum changes due to the mixing ratio of the two types of NPs are reasonably explained by the island domain formations composed of 10-nm AuNPs in the 5-nm AgNP matrix phase. Unexpectedly, the LSPR bands of adjacent AuNPs and AgNPs were *not* coupled, in contrast to the homologous NP system. This result is advantageous for the construction of complex plasmonic superstructures with various types of metallic NPs as the building blocks because the LSPR bands excited in the local space can be retained instead of *merging* with the neighbouring foreign particles (if the particles are not 'chemically' bonded[32,33]).

Fluorescence quenching experiments revealed that AuNPs maintain a high quenching efficiency against Cy3 dyes such that AuNPs in the mixed films can quench approximately

two times as much surface area. This high efficiency is due to the overlap of the LSPR band with the dye spectra.

The formation of AuNP island domains that are less than 100 nm in diameter suggests the possibility of the excitation of 'wavelength-tuned' LSPR in a limited nanospace from the bottom-up via the self-assembly technique. Various applications are possible using these nanoheterostructures.

Supporting Information

Supporting Information is available from the Wiley Online Library or from the author.

Acknowledgements

This study was supported by the NEXT Program, JSPS KAKENHI grant number 26246005 in Japan and the cooperative research program of the 'Network Joint Research Center for Materials and Devices'.

References

1 A. Taleb, C. Petit, M. P. Pileni, *J. Phys. Chem. B* 1998, **102**, 2214.

2 J. E. Millstone, S. J. Hurst, G. S. Métraux, J. I. Cutler, C. A. Mirkin, *Small* 2009, **5**, 646.

3 N. G. Bastús, F. Merkoçi, J. Piella, V. Puntes, *Chem. Mater*. 2014, **26**, 2836.

4 F. Kretschmer, S. Mühlig, S. Hoeppener, A. Winter, M. D. Hager, C. Rockstuhl, T. Pertsch, U. S. Schubert, *Part. Part. Syst. Charact*. 2014, **31**, 721.

5 D. Rodríguez-Fernández, L. M. Liz-Marzán, *Part. Part. Syst. Charact.* 2013, **30**, 46.

6 K. A. Willets, R. P. Van Duyne, *Ann. Rev. Phys. Chem*. 2007, **58**, 267.

7 P. K. Jain, HX. Huang, I. H. El-Sayed, M. A. El-Sayd, *Acc. Chem. Res*. 2008, **41**, 1578. A.

8 J. Cao, T. Sun, K. T. V. Grattan, *Sens. Actuators B* 2014, **195**, 332.

9 A. L. Feng, M. L. You, L. Tian, S. Singamaneni, M. Liu, Z. Duan, T. J. Lu, F. Xu, M. Lin, *Sci. Rep*. 2015, **5**, 7779.

10 M. A. Shenashen, S. A. El-Safty, E. A. Elshehy, *Part. Part. Syst. Charact.* 2014, **31**, 293.

11 S-H. Jeong, H. Choi, J. Y. Kim, T-W. Lee, *Part. Part. Syst. Charact*. 2015, **32**, 164.

12 C. L. Haynes, A. D. McFarland, LL. Zhao, R. P. Van Duyne, G. C. Schatz, L. Gunnarsson, J. Prikulis, B. Kasemo, M. Käll, *J. Phys. Chem. B*, 2003, **107**, 7337.

13 M. Toma, K. Toma, K. Michioka, Y. Ikezoe, D. Obara, K. Okamoto, K. Tamada, *Phys. Chem. Chem. Phys.* 2011, **13**, 7459.

14 K. Okamoto, B. Lin, K. Imazu, A. Yoshida, K. Toma, M. Toma, K. Tamada, *Plasmonics* 2012, **8**, 581.

15 S. J. Barcelo, A. Kim, W. Wu, Z. Li, *ACS Nano* 2012, **6**, 6446.

16 A. Vial, A.-S. Grimault, D. Macías, D. Barchiesi and M. L. de la Chapelle, *Phys. Rev. B,* 2005, **71**, 085416.

17 A. Yoshida, K. Imazu, X. Li, K. Okamoto, K. Tamada, *Langmuir* 2012, **28**, 17153.

18. H. Acharya, J. Sung, B.-H. Sohn, D. H. Kim, K. Tamada, C. Park, *Chem. Mater.* 2009, **21**, 4248.

19 J. N. Israelachvili*, Intermolecular and Surface Forces*, 3rdedition, Elsevier, MA, USA2011.

20 W. B. Russel. D. A. Saville, W. R. Schowalter, *Colloidal Dispersions*, Cambridge University Press, Cambridge, UK 1989.

21 Y. Ikezoe, S. J. Kim, I. Yamashita, M. Hara, *Langmuir* **2009**, 25, 4293.

22 E. A. Jares-Erijman, T. M. Jovin, *Nature Biotech.* 2003, **21**, 1387.

23 S. Mayilo, M. A. Kloster, M. Wunderlich, A. Lutich, T. A. Klar, A. Nichtl, K. Kürzinger, F. D. Stefani, J. Feldmann, *Nano Lett.* 2009, **9**, 4558.

24 A. Samanta, Y. Zhou, S. Zou, H. Yan, Y. Liu, *Nano Lett*. 2014, **14**, 5052.

25 X. Zhang, C. A. Marocico, M. Lunz, V. A. Gerard, Y. K. Gun´ko, V. Lesnyak, N. Gaponik, A. S. Susha, A. L. Rogach, A. L. Bradley, *ACS Nano* 2014, **8**, 1273.

26 E. Dulkeith, A.C. Morteani, T. Niedereichholz, T. A. Klar, J. Feldmann, S. A. Levi, F. C. J. M. van Veggel, D. N. Reinhoudt, M. Möller, D. I. Gittins, *Phys. Rev. Lett.* 2002, **89**, 203002.

27 E. Usukura, S. Shinohara, K. Okamoto, J. Lim, K. Char, K. Tamada, *Appl. Phys. Lett.* 2014, **104**, 121906.

28 X. Cui, K. Tawa, K. Kintaka, J. Nishii, *Adv. Func. Mater*. 2010, **20**, 945.

29 Y. Chen, K. Munechika, D. S. Ginger, *Nano Lett.* 2007, **7**, 690.

30 M. P. Singh, G. F. Strouse, *J. Am. Chem. Soc.* 2010, *132,* 9383.

31 S. Chowdhury, Z. Wu, A. Jaquins-Gerstl, S. Liu, A. Dembska, B. A. Armitage, R. Jin, L. A. Peteanu, *J. Phys. Chem. C* 2011, **115**, 20105.

32 S. W. Verbruggen, M. Keulemans, J. A. Martens, S. Lenaerts, *J. Phys. Chem. C* 2013, **117**, 19142.

33 H. Liu, M. Shen, J. Zhao, R. Guo, X. Cao, G. Zhang, X. Shi, *Coll. Surf. B: Biointerfaces* 2012, **94**, 58.

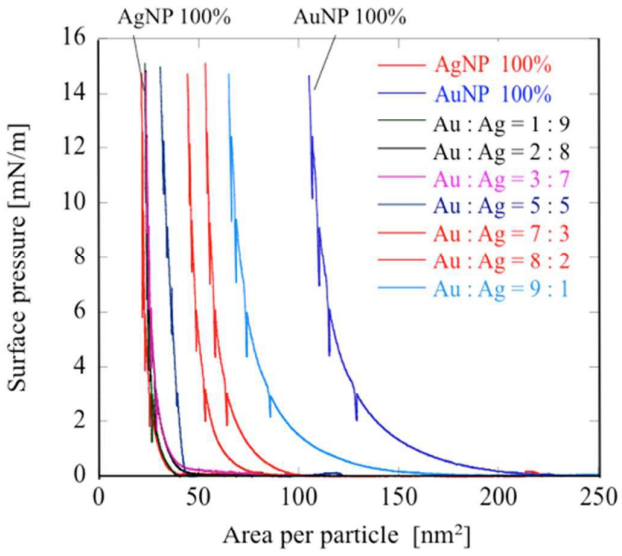

Mixing Ratio Au : Ag	1:9	2:8	3:7	5:5	7:3	8:2	9:1
Area per particle (nm^2)							
Theoretical value	29	31	34	42	62	70	90
Experimental value	30	30	33	45	58	66	85

Figure 1. Surface pressure (Π) - Area (A) curves of 5-nm AgNP and 10-nm AuNP mixed monolayers.

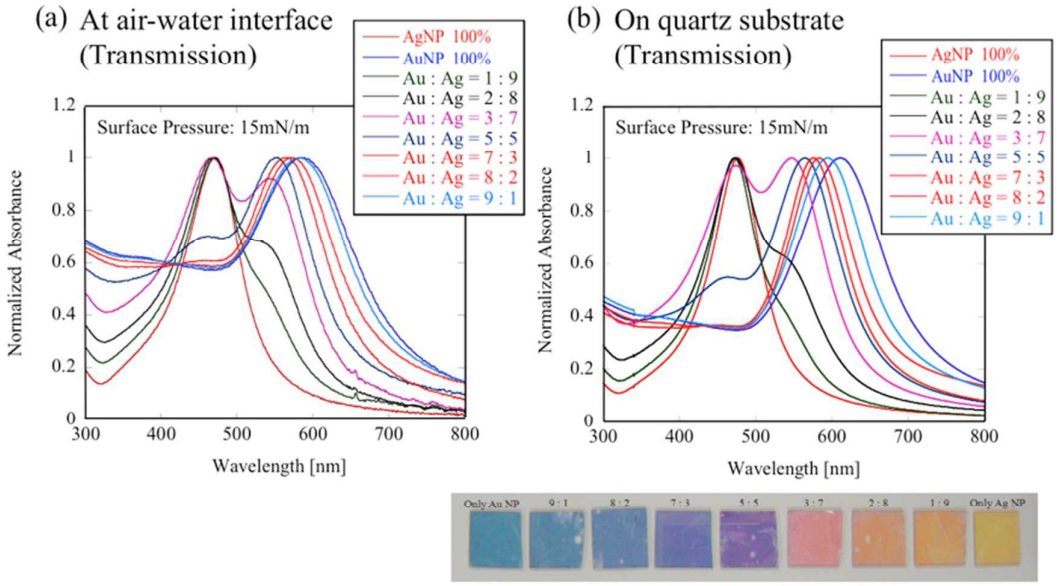

Figure 2. Normalized absorption spectra of 5-nm AgNP and 10-nm AuNP mixed monolayers at the air-water interface (a) and on a quartz substrate (b). The colour of the AgNP/AuNP mixed films can be confirmed in the photograph below (the size of the substrates are 2 cm x 2 cm).

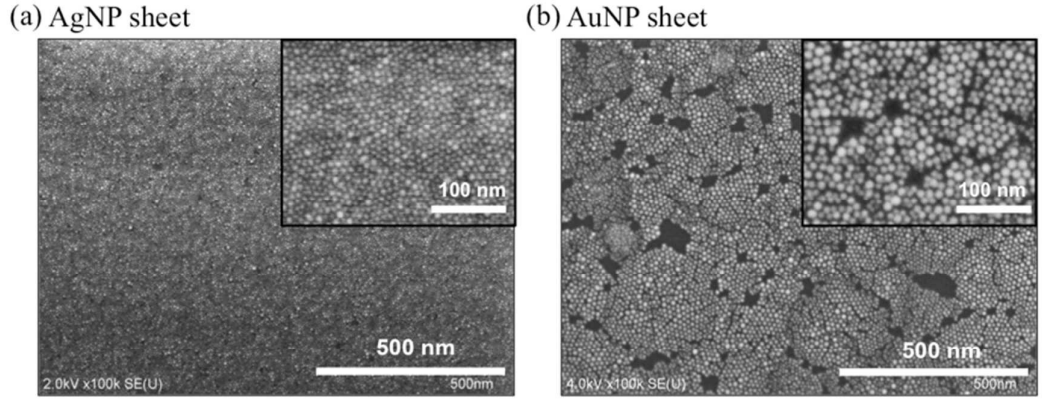

Figure 3. SEM images of single component 5-nm AgNP (a) and 10-nm AuNP (b) monolayers.

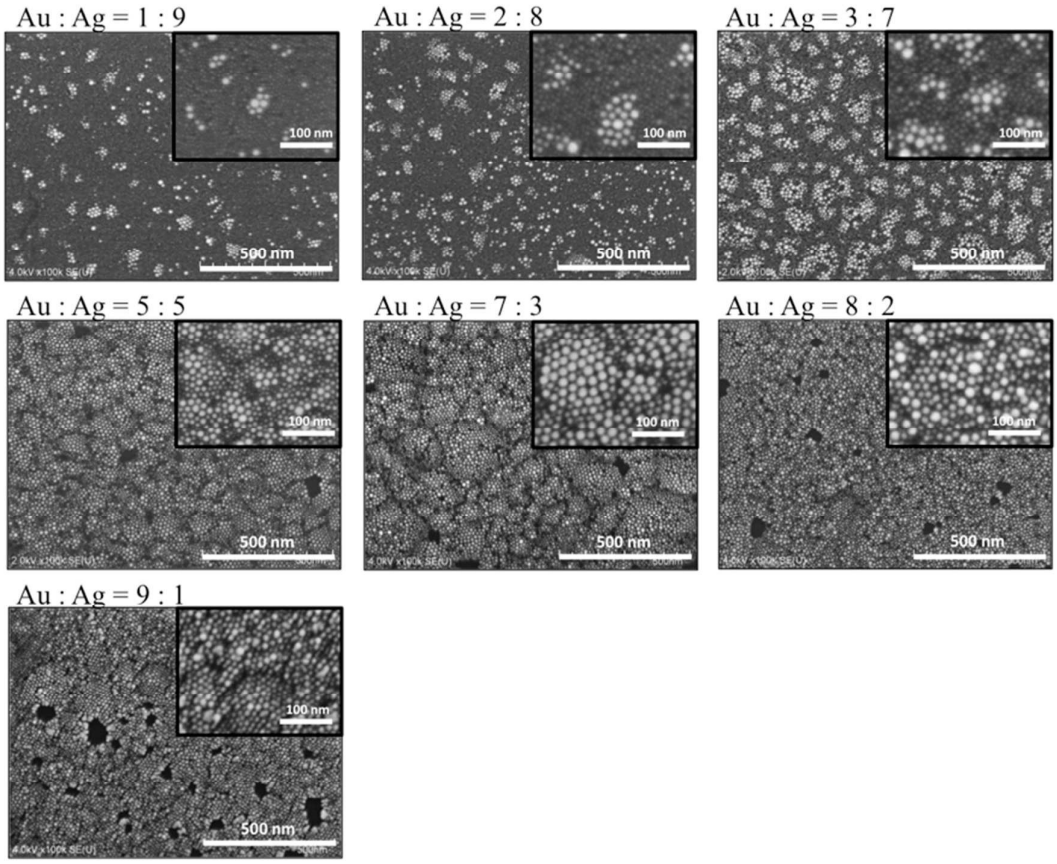

Figure 4. SEM images of 5-nm AgNP and 10-nm AuNP mixed monolayers.

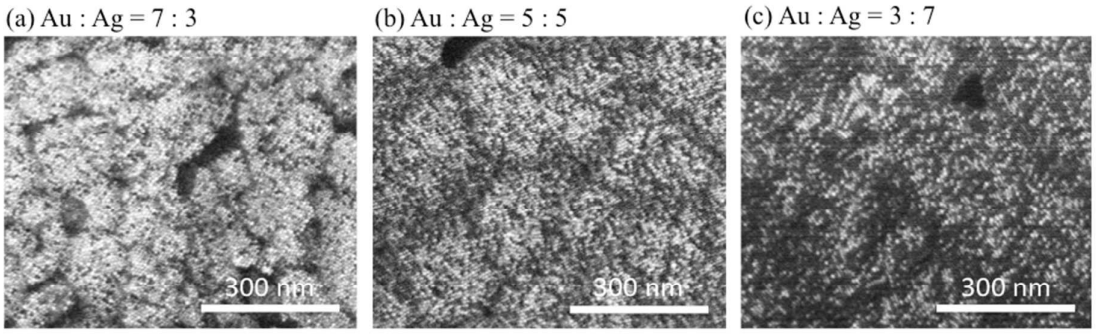

Figure 5. SEM images of 5-nm AgNP and 5-nm AuNP mixed monolayers.

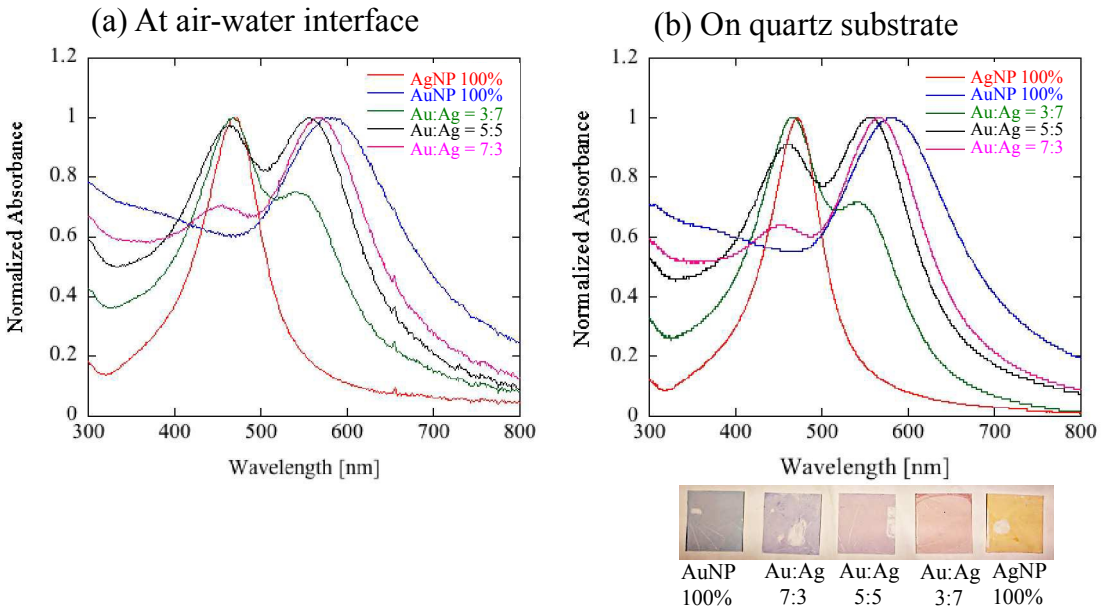

Figure 6. Normalized absorption spectra of 5-nm AgNP and 5-nm AuNP mixed monolayers at the air-water interface (a) and on a quartz substrate (b).

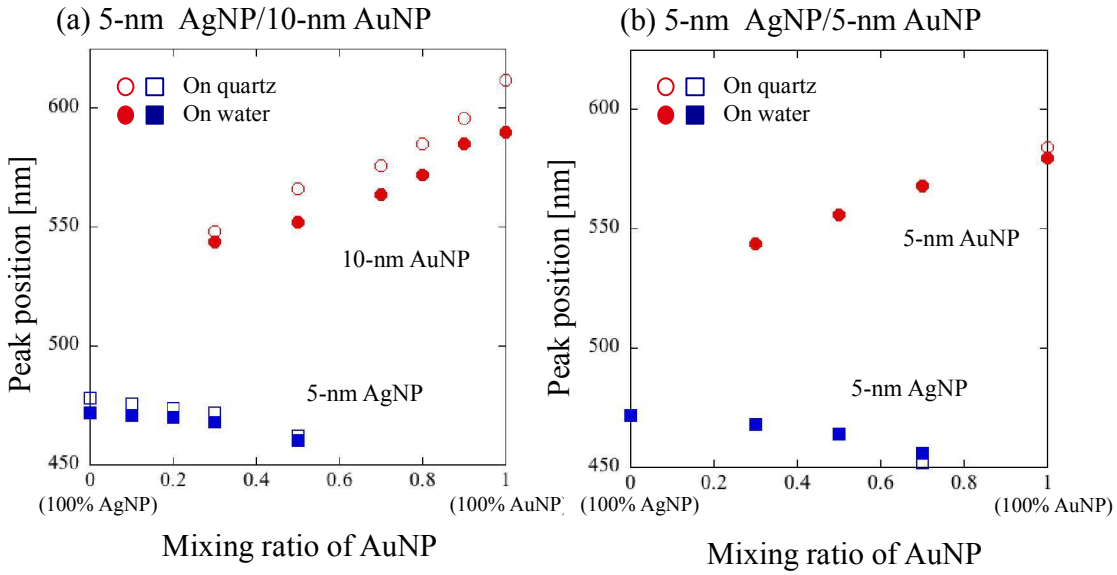

Figure 7. LSPR peak positions originating from AgNP and AuNP in the mixed film on water (solid mark) and on quartz substrate (open mark); (a) 5-nm AgNP and 10-nm AuNP mixed films (the data from Figure 2), (b) 5-nm AgNP and 5-nm AuNP mixed films (the data from Figure 6).

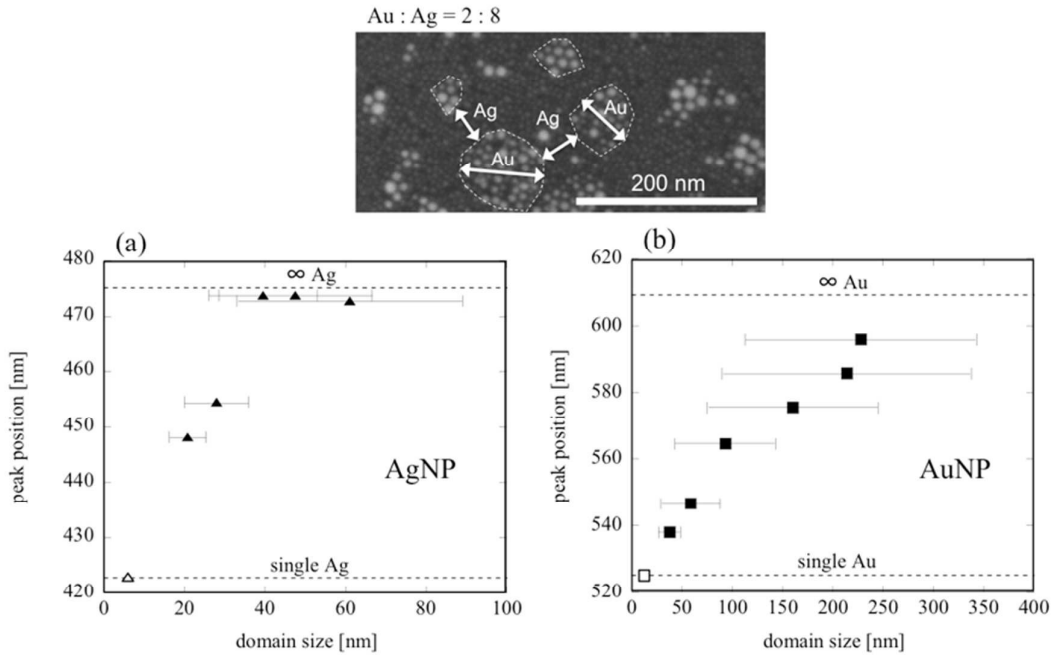

Figure 8. Correlation between domain size and LSPR peak position; (a) 5-nm AgNP matrix phase, (b) 10-nm AuNP island. The band positions were determined from the data in Figure 2b.

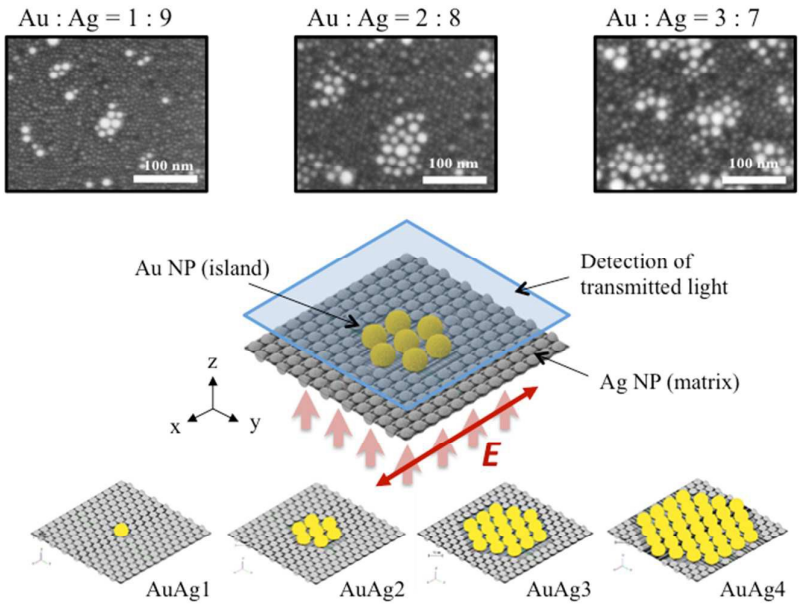

Figure 9. Model of 5-nm AgNP and 10-nm AuNP mixed film for FDTD simulation based on the experimental results (AuAg1, AuAg2, AuAg3, and AuAg4).

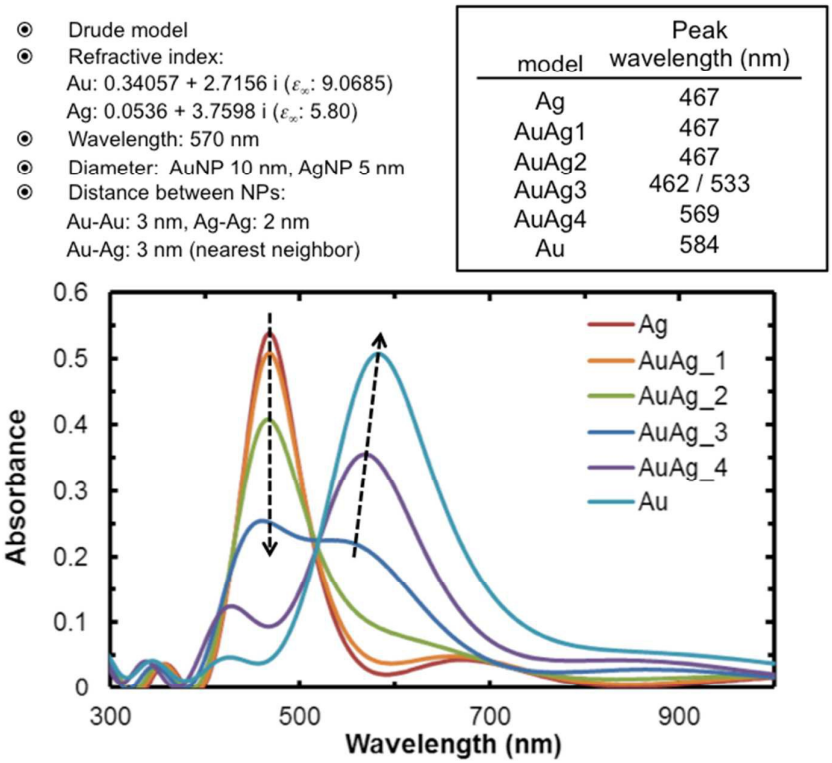

Figure 10. Absorption spectra of a 5-nm AgNP and 10-nm AuNP mixed sheet obtained by FDTD simulation (AuAg1, AuAg2, AuAg3, and AuAg4).

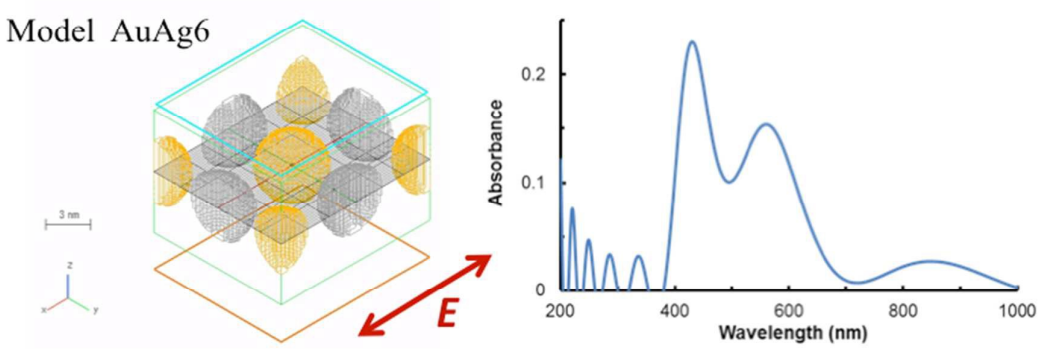

Figure 11. Model of alternately aligned 5-nm AgNPs and 5-nm AuNPs (AuAg6) for FDTD simulation and resulting absorption spectrum.

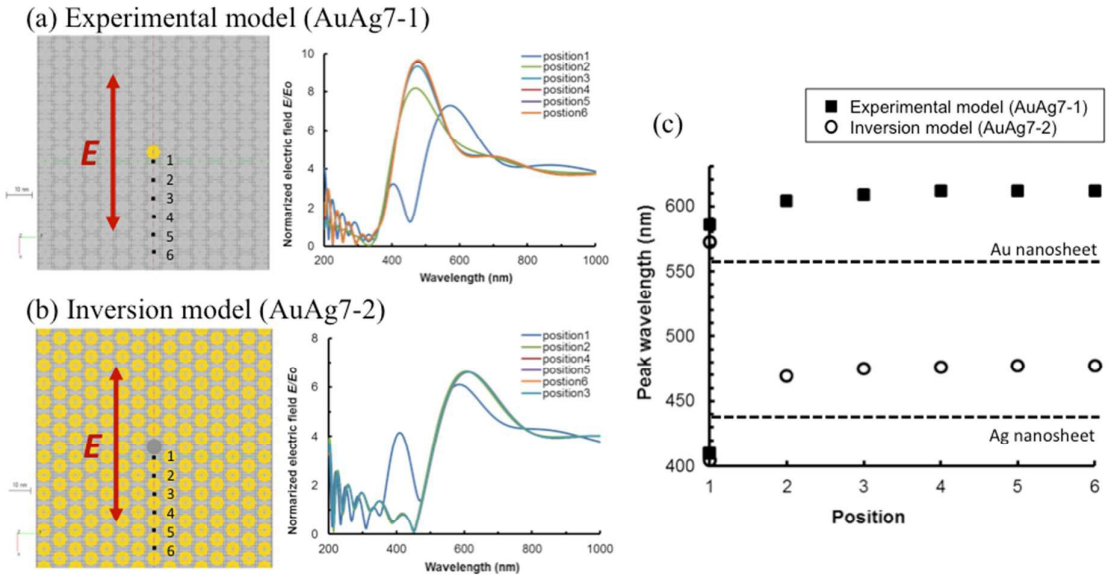

Figure 12. FDTD simulation of (a) experimental model (AuAg7-1) and (b) inversion model (AuAg7-2), with a single particle located in the hexagonally packed 2D sheet (5-nm AgNP and 5-nm AuNP, gap distance: 2 nm). The local E-field intensity normalized by irradiated light intensity (E/E_0) at each gap position (positions 1 - 6) predicts the 'local' absorption spectrum. The obtained LSPR peak wavelengths are summarized in (c).

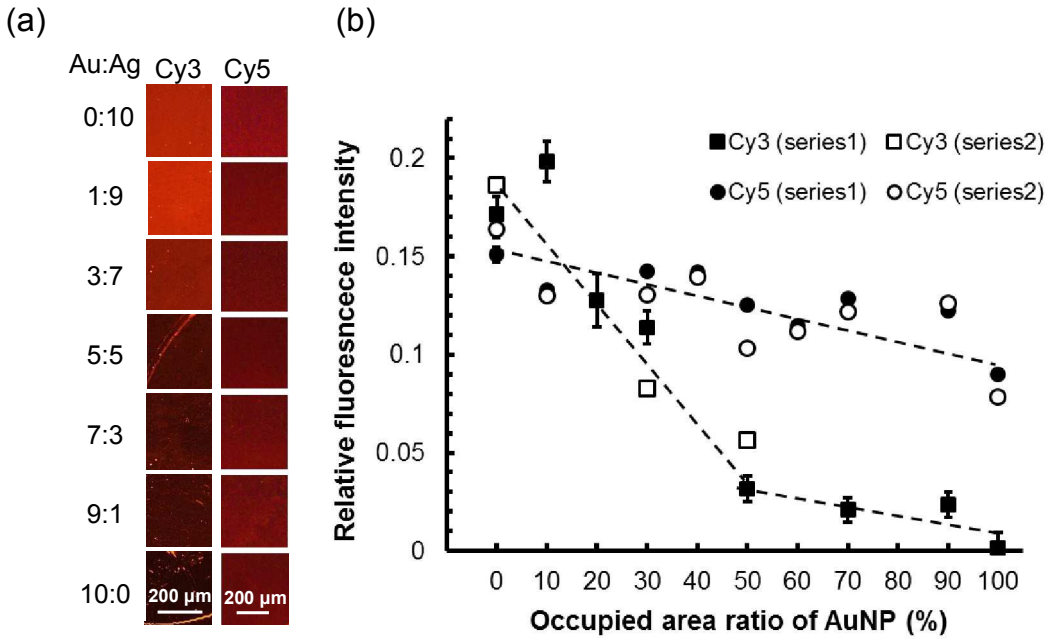

Figure 13. Fluorescence microscopy images of Cy3- and Cy5-labelled surfaces on 5-nm AgNP and 10-nm AuNP mixed monolayers (a) and the plot of relative fluorescence intensity against area occupied by the AuNP (b).

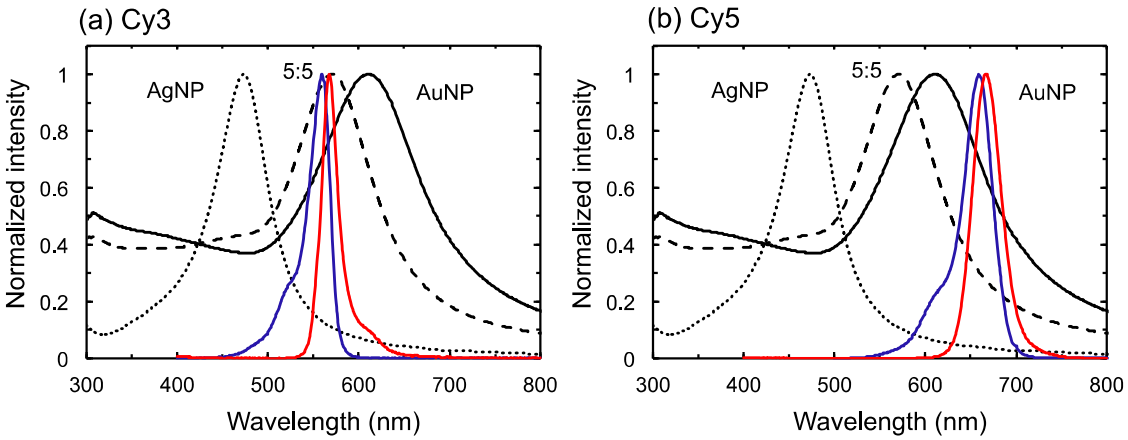

Figure 14. Absorption spectra of single component 5-nm AgNP (dotted line) and 10-nm AuNP (solid line) sheets and 5:5 mixed sheet (dashed line) presented together with Ex/Em spectra of Cy3 (a) and Cy5 (b).

Table of contents

AuNPs form ~100-nm island domains in a homogeneous AgNPs matrix phase in mixed monolayers, which maintain independent LSPR bands and selective fluorescence quenching.